ADVANCED MATERIALS

Supporting Information

for *Adv. Mater.,* DOI: 10.1002/adma.202109416

Mechanically Guided Hierarchical Assembly of 3D Mesostructures

Hangbo Zhao, Xu Cheng, Changsheng Wu, Tzu-Li Liu, Qinai Zhao, Shuo Li, Xinchen Ni, Shenglian Yao, Mengdi Han, Yonggang Huang, Yihui Zhang,* and John A. Rogers**

WILEY-VCH

Supporting Information

Mechanically guided hierarchical assembly of 3D mesostructures

Hangbo Zhao, Xu Cheng, Changsheng Wu, Tzu-Li Liu, Qinai Zhao, Shuo Li, Xinchen Ni, Shenglian Yao, Mengdi Han, Yonggang Huang, Yihui Zhang*, John A. Rogers**

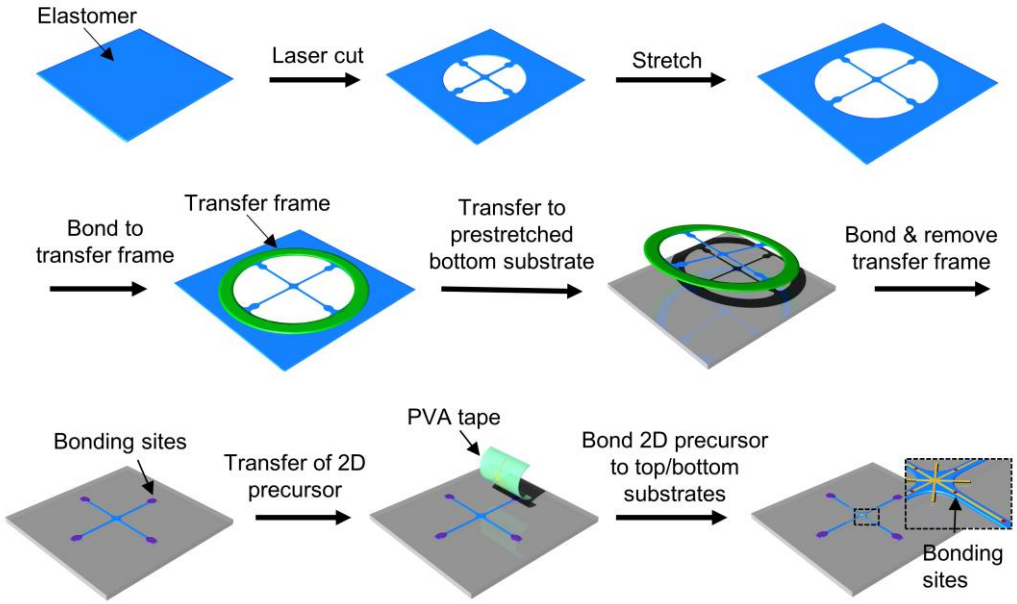

Figure S1. Schematic illustration of steps for fabricating 2D precursors bonded on two levels of independently prestretched elastomeric substrates.

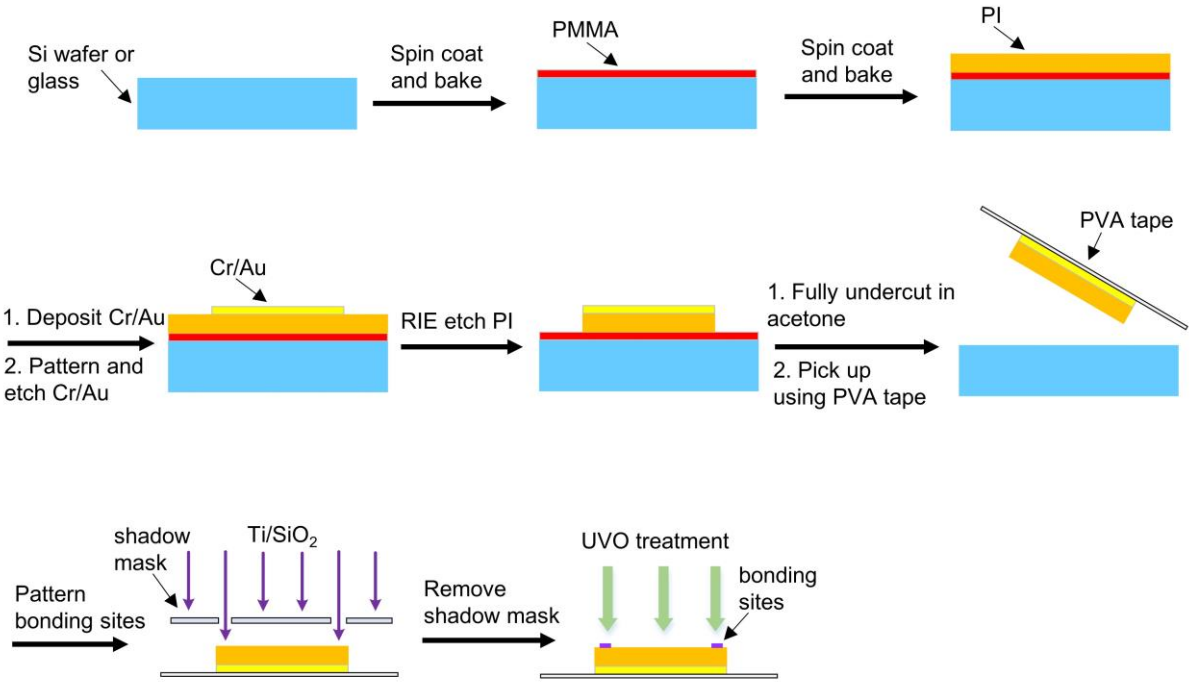

Figure S2. Schematic illustration of steps for fabricating 2D precursors with patterned bonding sites.

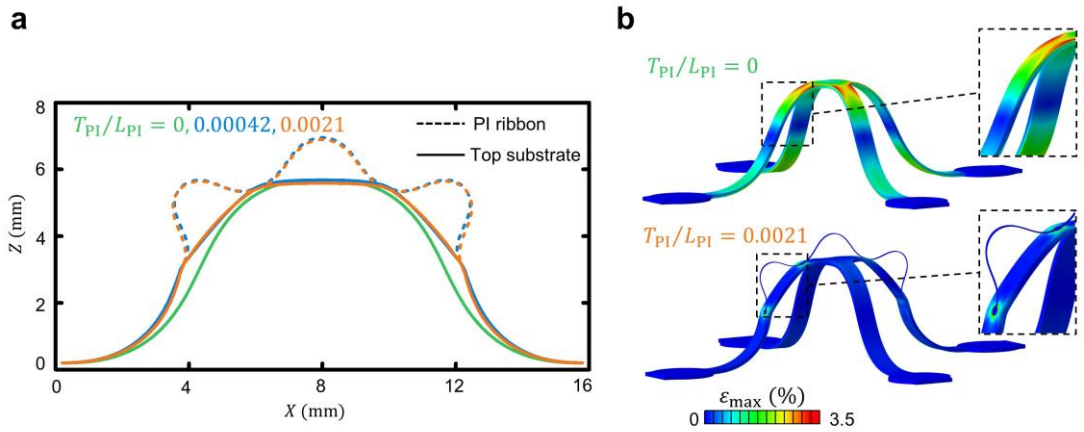

Figure S3. FEA results for the distributions of a) coordinate and b) maximum principal strain of a representative hierarchical 3D mesostructure with different dimensionless PI thicknesses (T_{PI}/L_{PI}).

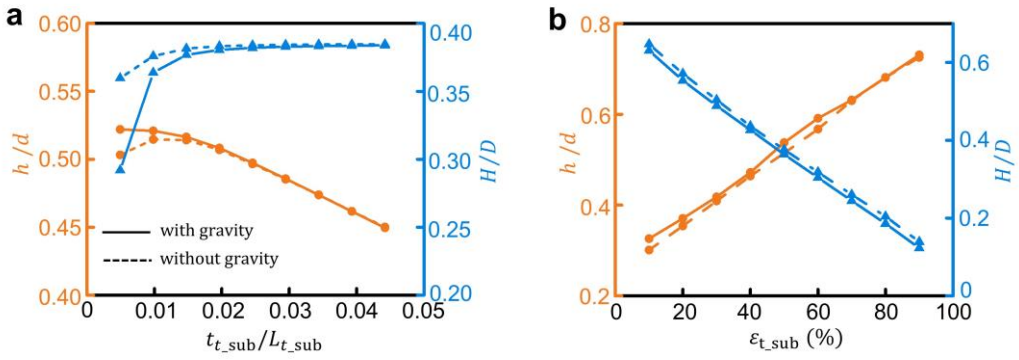

Figure S4. FEA results for the dependence of dimensionless heights of a basic hierarchical 3D mesostructure shown in Figure 1a on the a) dimensionless thickness and b) prestrain of the top substrate with and without considering gravity.

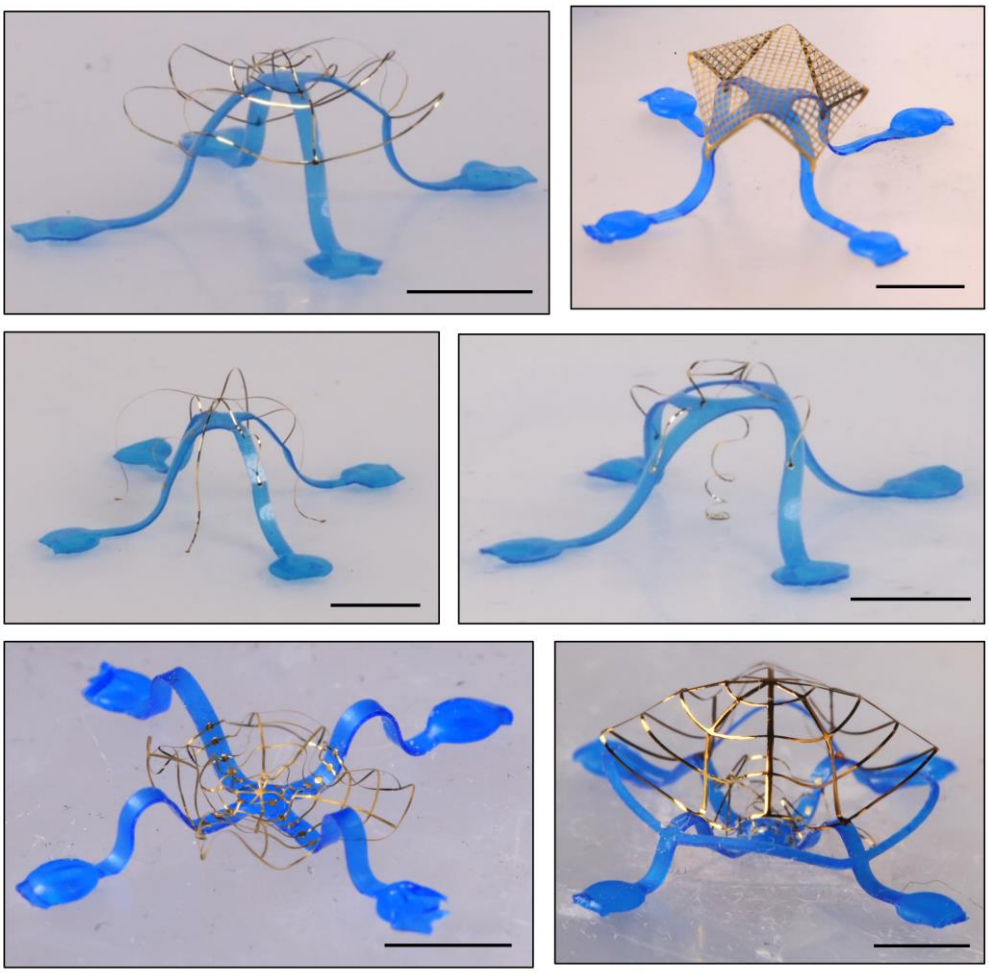

Figure S5. Optical images of selected 3D mesostructures shown in Figure 2 and 3 with higher magnification. Scale bars, 5 mm.

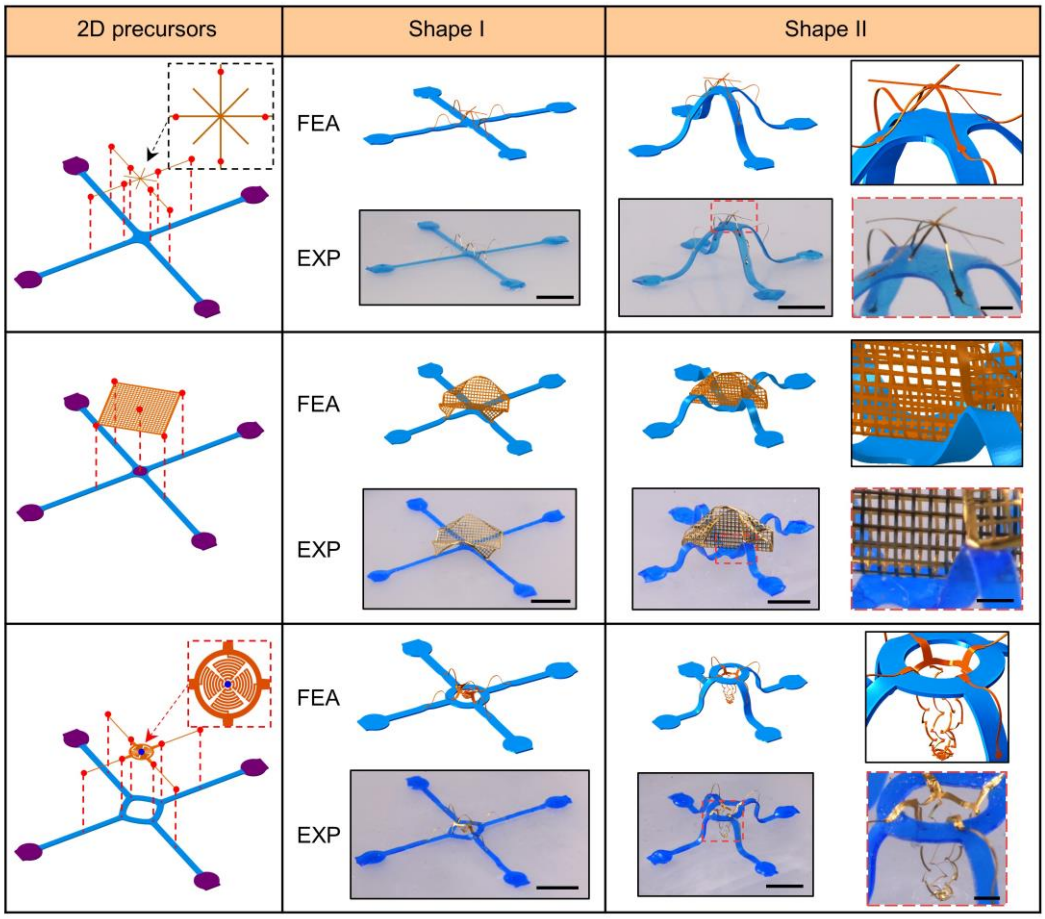

Figure S6. 2D geometries, FEA predictions and experimental results (optical images) of several 3D mesostructure designs, including a flat cross supported by buckled ribbons on a buckled cross substrate, a square mesh folded by a concave cross substrate, and a mesh basket supported by table-like structure with a ring top. Shape I and Shape II correspond to the shapes formed after the Stage I and Stage II assembly steps. The right column in Shape II shows enlarge views of selected regions. Scale bars, 5 mm in solid boxes and 1 mm in dashed boxes.

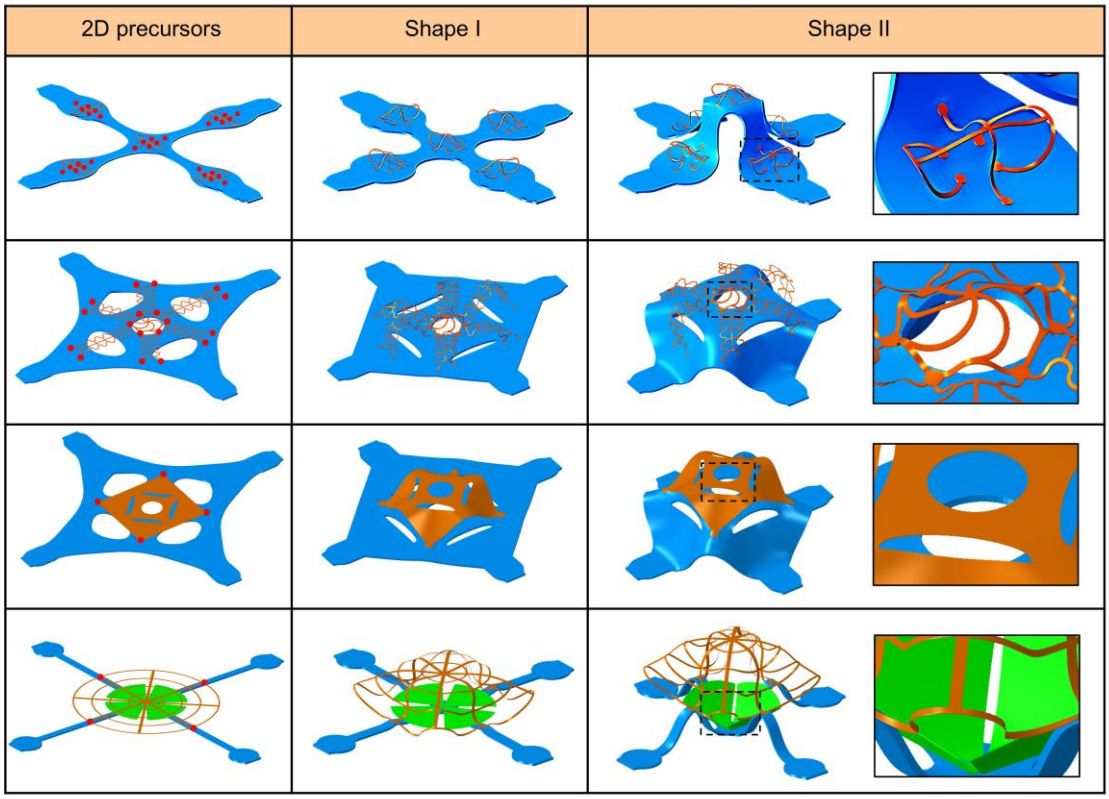

Figure S7. 2D geometries and FEA predictions of 3D mesostructure designs with different 2D precursor/top substrate layouts and bonding site arrangements. Shape I and Shape II correspond to the shapes formed after the Stage I and Stage II assembly steps. The right column in Shape II shows enlarge views of selected regions.

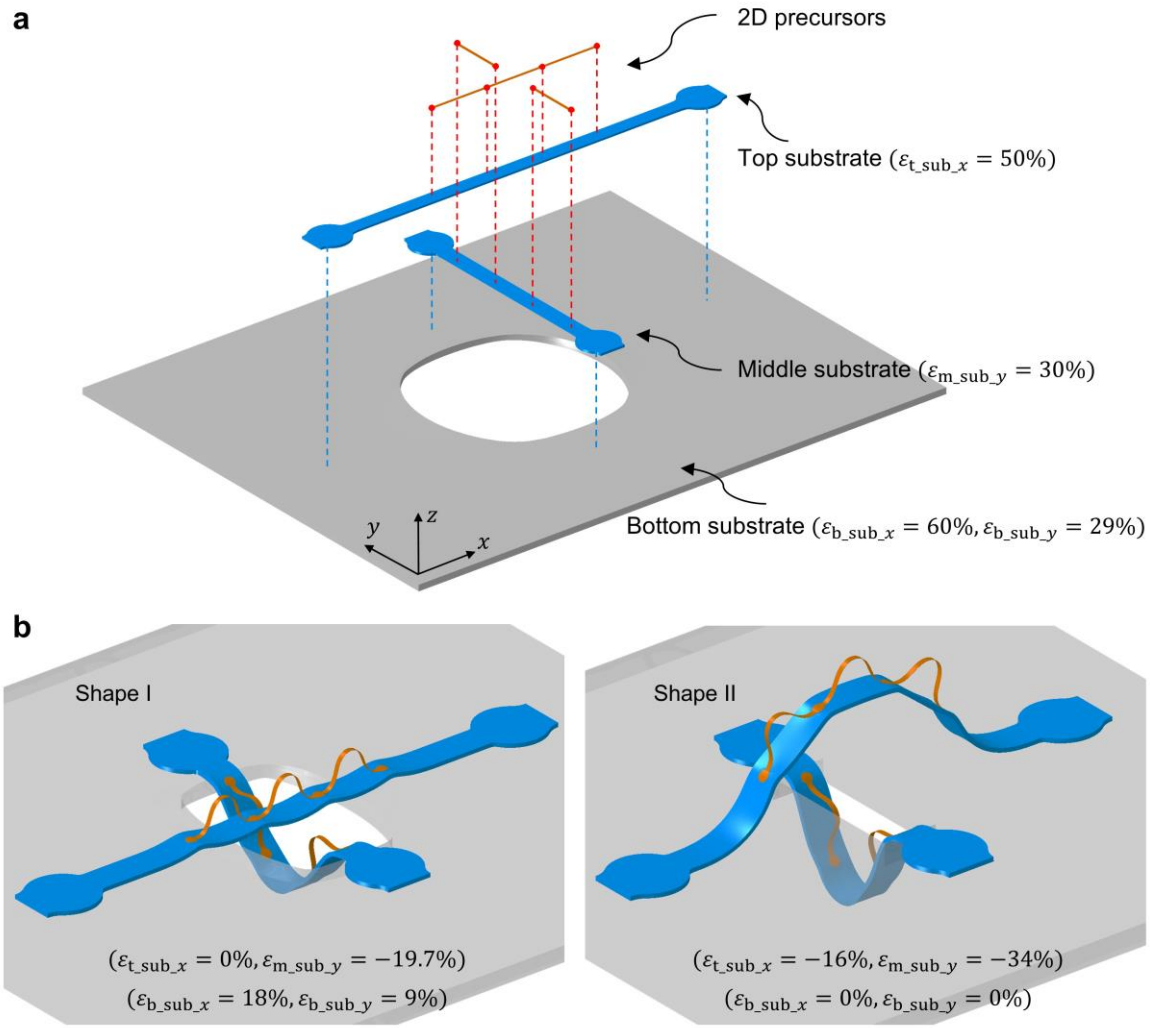

Figure S8. FEA results of a 3D hierarchical mesostructure with buckling deformations selectively directed to both sides of the elastomeric substrate. (a) An exploded-view illustration of the 2D state of the 3D hierarchical mesostructure. The top, middle and bottom substrates are prestretched with $\varepsilon_{t\_sub\_x} = 50\%$, $\varepsilon_{m\_sub\_y} = 30\%$, and $(\varepsilon_{b\_sub\_x}, \varepsilon_{b\_sub\_y}) = (60\%, 29\%)$, respectively. (b) FEA results for the deformed configurations (Shape I and Shape II) of the 3D hierarchical mesostructure. Shape I and Shape II correspond to 3D configurations with complete release of prestrain in top substrate (i.e., $\varepsilon_{t\_sub\_x} = 0\%$), and complete release of prestrain in bottom substrate (i.e., $\varepsilon_{b\_sub\_x} = \varepsilon_{b\_sub\_y} = 0\%$), respectively.

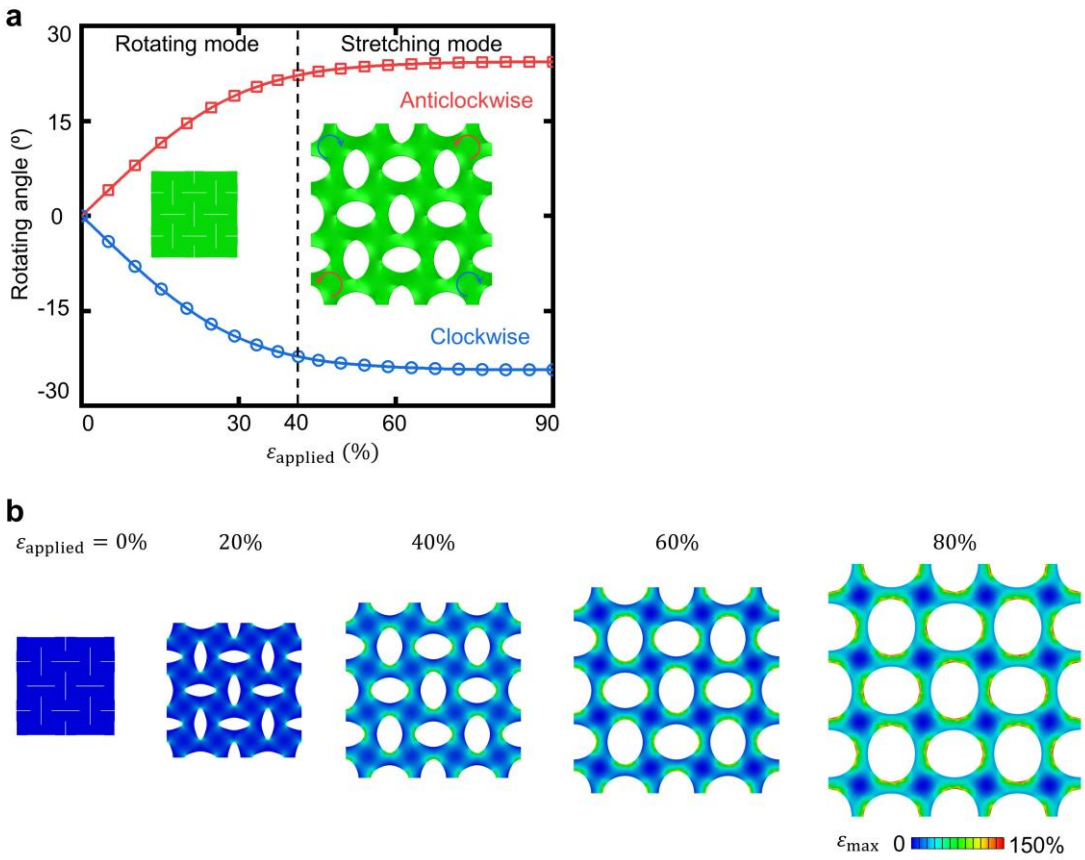

Figure S9. a) Plot of the rotation angles at the centers of an individual square unit in a typical kirigami elastomer substrate used in this study as a function of the applied biaxial strain. b) Color representations of the distributions of the maximum principal strain in the kirigami substrate used in this study with different biaxial prestrain.

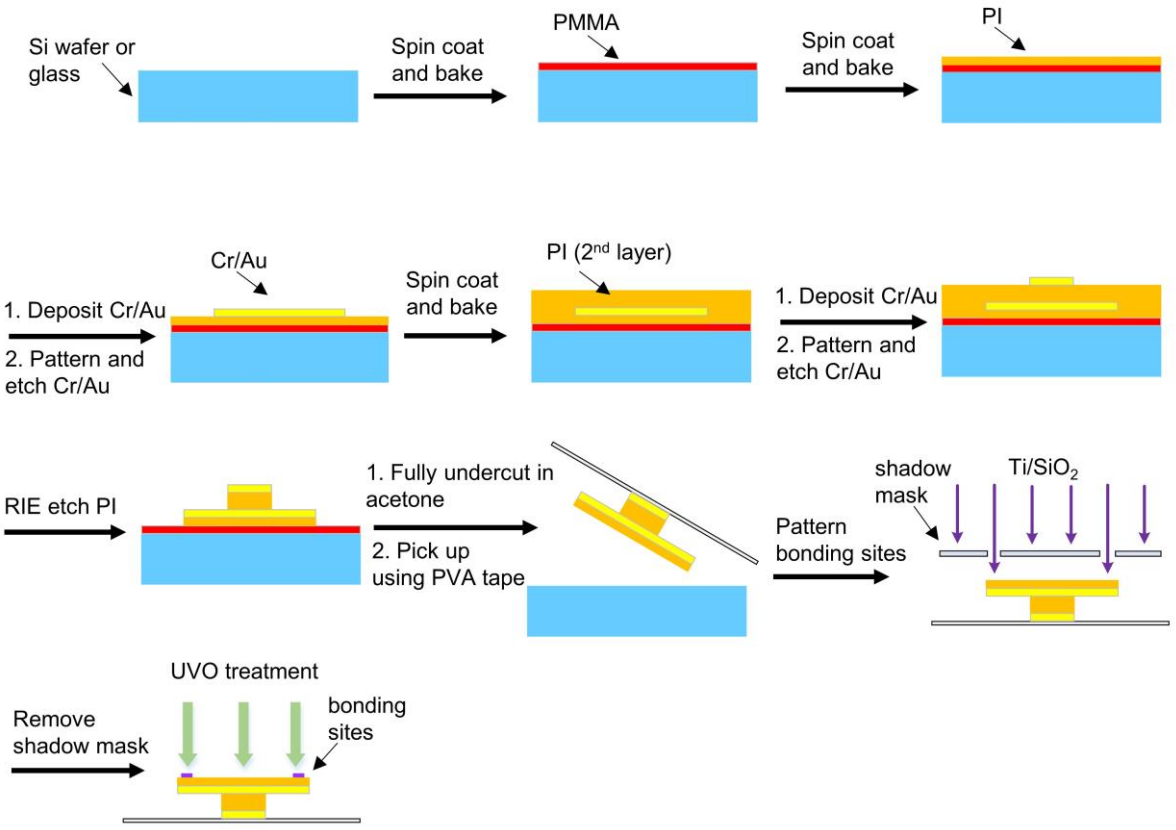

Figure S10. Schematic illustration of steps for fabricating 2D precursors for origami-inspired 3D mesostructures.

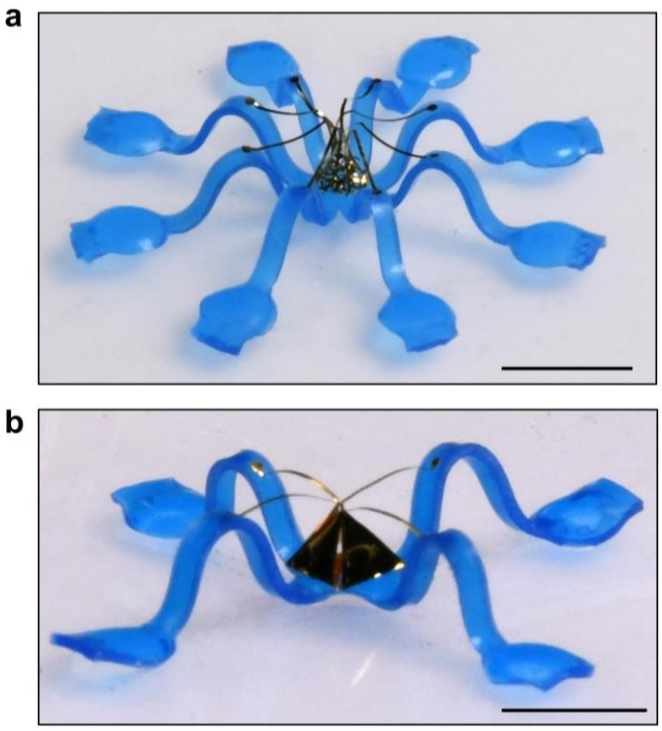

Figure S11. Optical images of the (a) 3D closed cage mesostructure and (b) 3D closed pyramid mesostructure shown in Figure 5a with higher magnification. Scale bars, 5 mm.

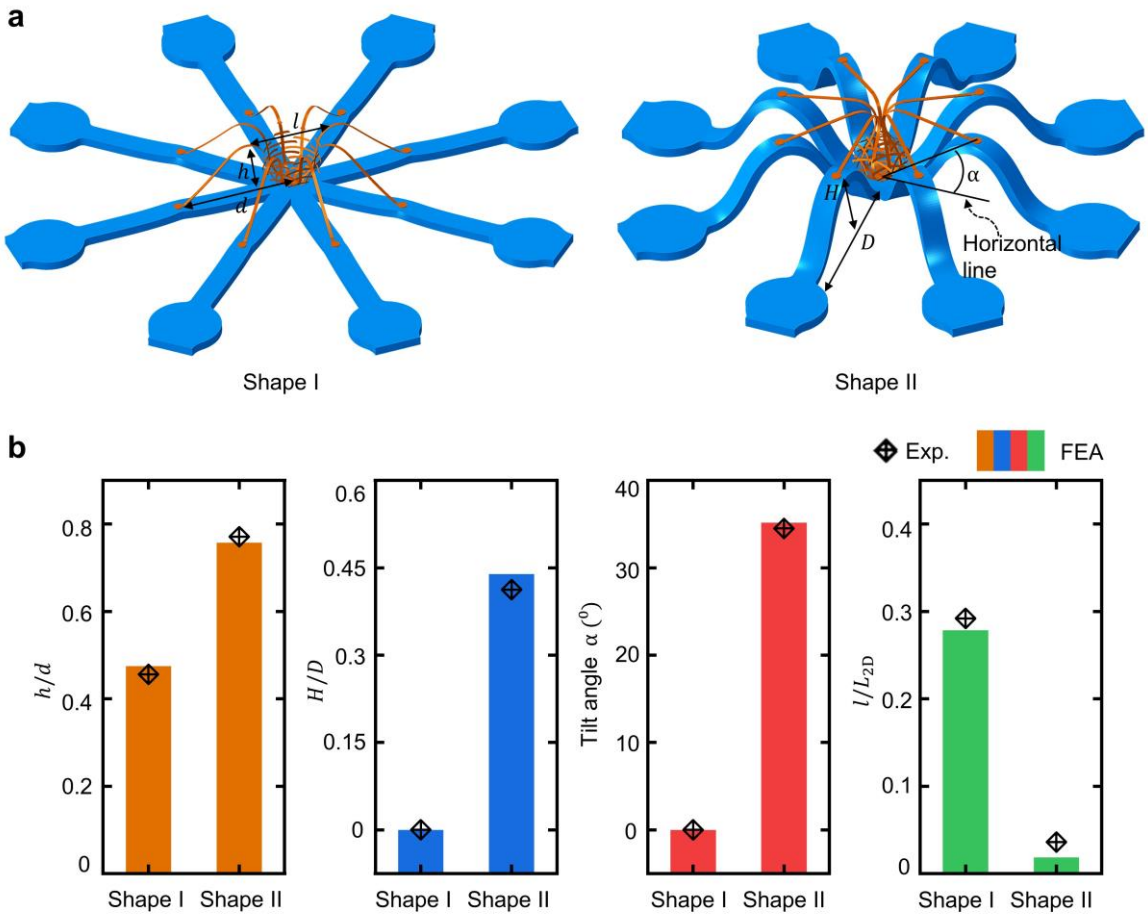

Figure S12. Quantitative geometric differences between Shape I and Shape II in the hierarchical assembly process for a 3D closed cage shown in Figure 5a. a) Schematic illustration of the key geometric parameters describing the 3D shapes of the cage. b) Quantitative comparisons of key geometric parameters of Shape I and Shape II of the 3D cage. Bar plots correspond to FEA results and star symbols correspond to experimental results.

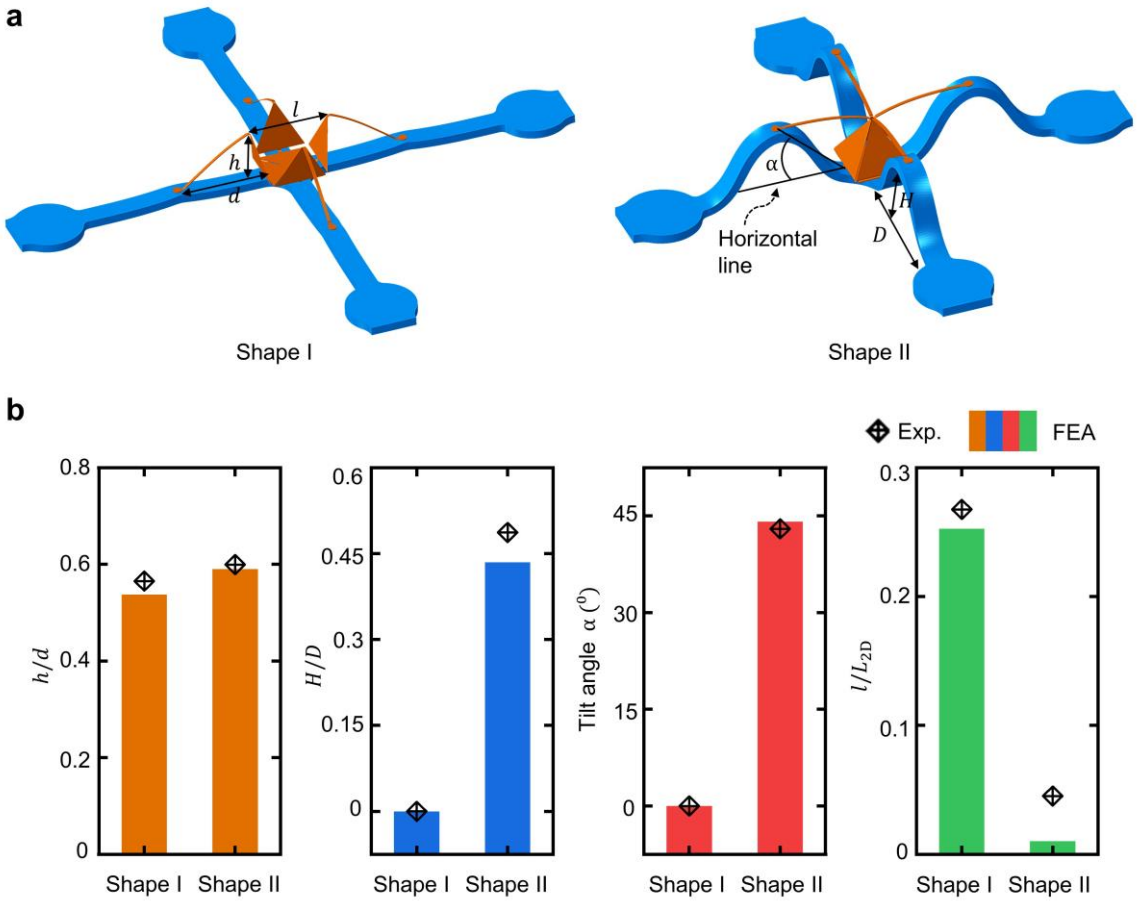

Figure S13. Quantitative geometric differences between Shape I and Shape II in the hierarchical assembly process for a 3D closed pyramid shown in Figure 5a. a) Schematic illustration of the key geometric parameters describing the 3D shapes of the cage. b) Quantitative comparisons of key geometric parameters of Shape I and Shape II of the 3D pyramid. Bar plots correspond to FEA results and star symbols correspond to experimental results.

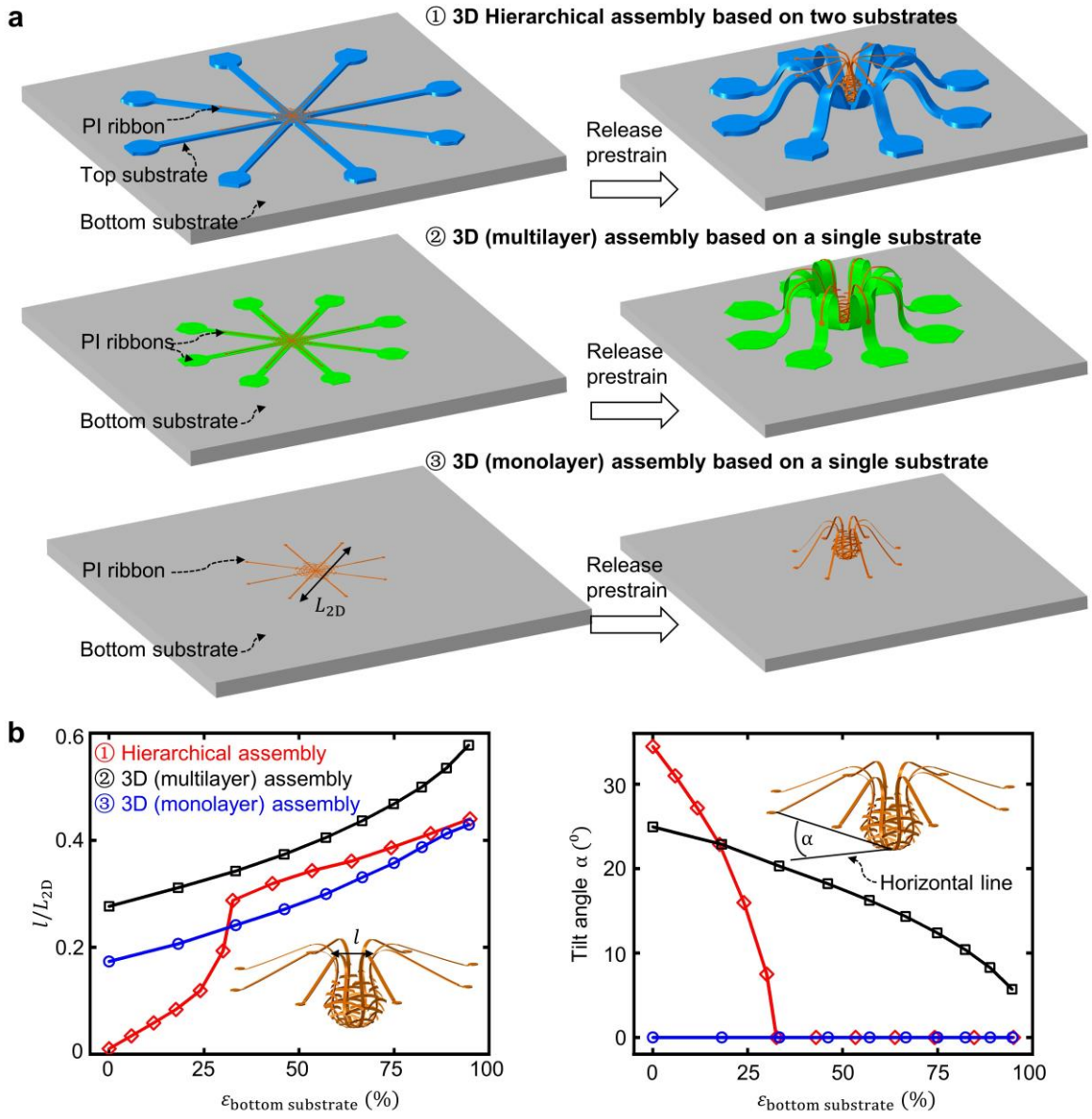

Figure S14. Different 3D cage geometries from hierarchical 3D assembly and from assembly on a single substrate. a) Schematic illustration of three different types of 3D assembly processes to form 3D cage structures: hierarchical assembly based on two substrates, 3D multilayer assembly based on a single substrate, and 3D monolayer assembly based on a single substrate. b) Quantitative differences of the degree of cage closeness (characterized by l/L_{2D}) and the tilt angle of the supporting ribbon α of the 3D cages formed by the three types of assembly processes in a).

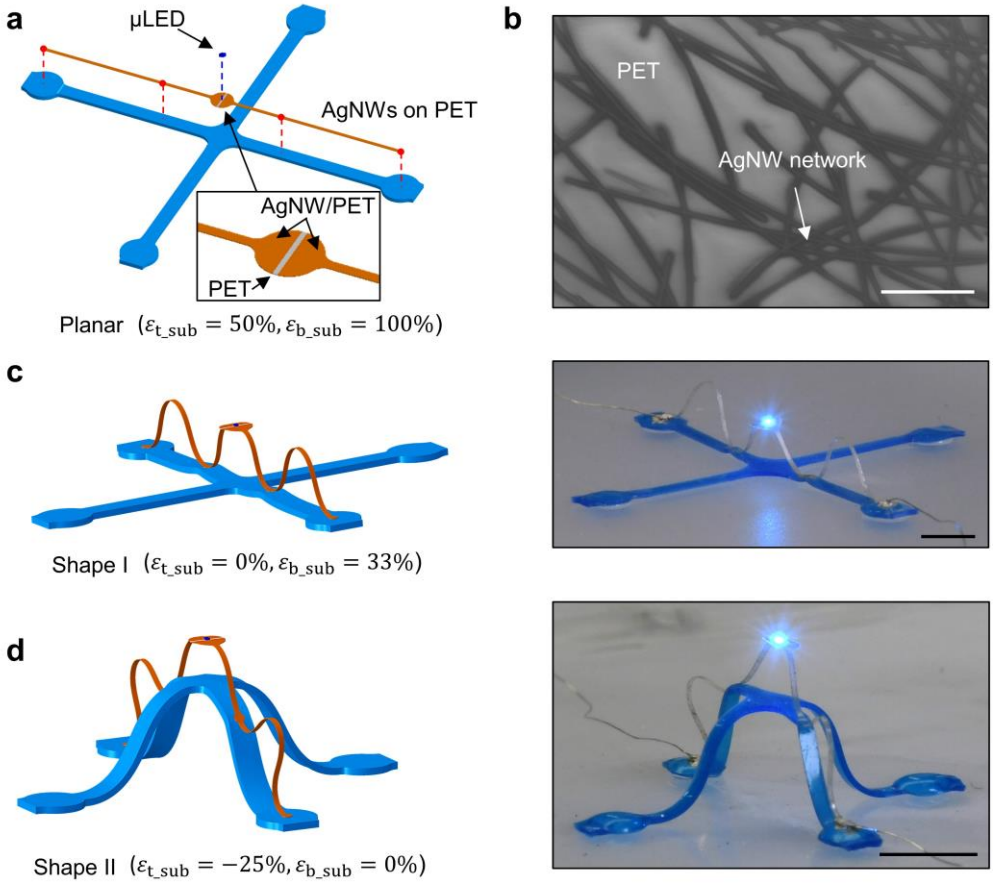

Figure S15. 3D hierarchical electrodes based on AgNW-coated PET. a) Schematic illustration of the 2D precursor, which includes a microscale LED assembled on a AgNW-coated PET ribbon. b) Scanning electron microscope (SEM) image of the AgNW network on the PET substrate after UV light-induced welding of AgNWs. c-d) FEA predictions and experimental results (optical images) of a 3D conductive ribbon formed by hierarchical assembly with the LED on. Scale bars, 5 μm in b and 5 mm in c and d.

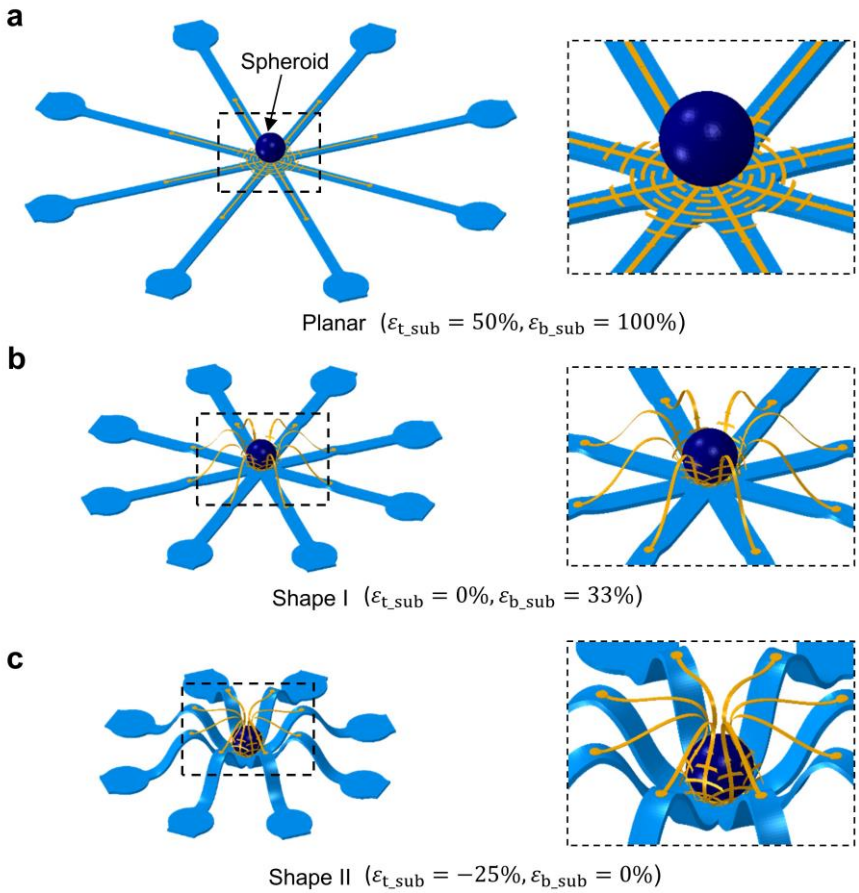

Figure S16. FEA predictions showing different stages of the mechanically guided hierarchical assembly process, which encloses a 3D mesh mesostructure around the surface of a spheroid: a) $\varepsilon_{t\_sub} = 50\%, \varepsilon_{b\_sub} = 100\%$; b) $\varepsilon_{t\_sub} = 0\%, \varepsilon_{b\_sub} = 33\%$; c) $\varepsilon_{t\_sub} = -25\%, \varepsilon_{b\_sub} = 0\%$.

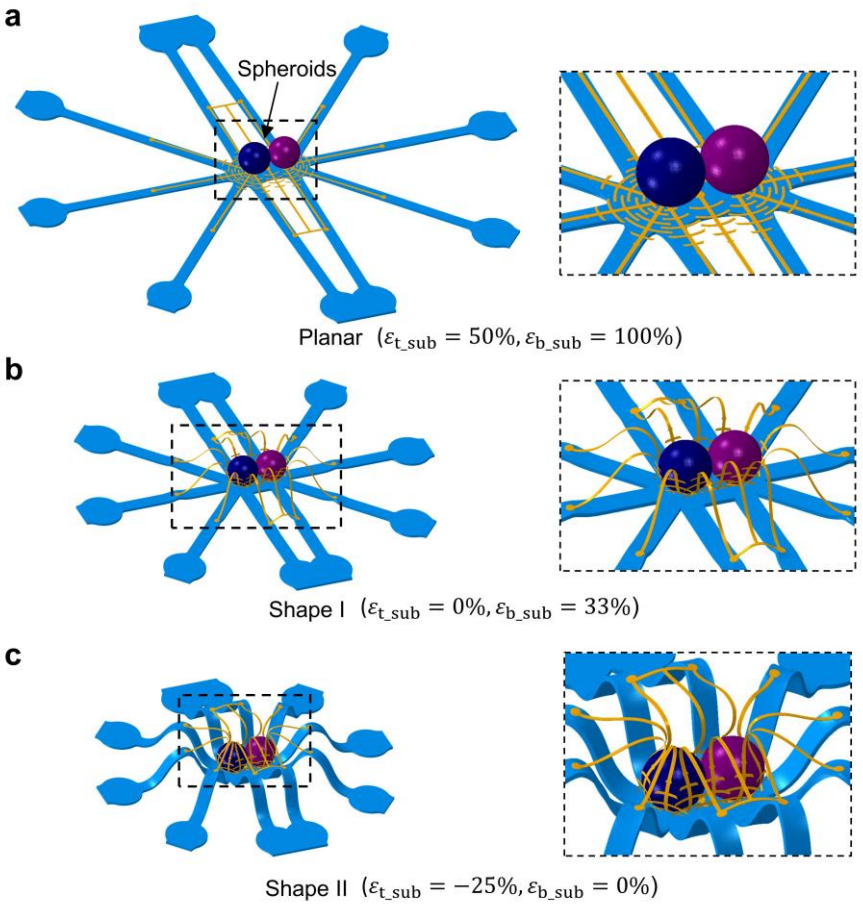

Figure S17. FEA predictions showing different stages of the process of enclosing a 3D mesh mesostructure around the surface of two spheroids in proximity: a) $\varepsilon_{t\_sub} = 50\%, \varepsilon_{b\_sub} = 100\%$; b) $\varepsilon_{t\_sub} = 0\%, \varepsilon_{b\_sub} = 33\%$; c) $\varepsilon_{t\_sub} = -25\%, \varepsilon_{b\_sub} = 0\%$.